University of South Carolina
Scholar Commons

8-1-2006

A Compact Digitally Controlled Fuel Cell/Battery Hybrid Power Source

Zhenhua Jiang
University of Miami, zjiang1@miami.edu

Roger A. Dougal
University of South Carolina - Columbia, dougal@engr.sc.edu

Follow this and additional works at: https://scholarcommons.sc.edu/elct_facpub

Part of the Electrical and Computer Engineering Commons

A Compact Digitally Controlled Fuel Cell/Battery Hybrid Power Source

Zhenhua Jiang, *Member, IEEE*, and Roger A. Dougal, *Senior Member, IEEE*

Abstract—A compact digitally controlled fuel cell/battery hybrid power source is presented in this paper. The hybrid power source composed of fuel cells and batteries provides a much higher peak power than each component alone while preserving high energy density, which is important and desirable for many modern electronic devices, through an appropriately controlled dc/dc power converter that handles the power flow shared by the fuel cell and the battery. Rather than being controlled to serve only as a voltage or current regulator, the power converter is regulated to balance the power flow to satisfy the load requirements while ensuring the various limitations of electrochemical components such as battery overcharge, fuel cell current limit (FCCL), etc. Digital technology is applied in the control of power electronics due to many advantages over analog technology such as programmability, less susceptibility to environmental variations, and low parts count. The user can set the FCCL, battery current limit, and battery voltage limit in the digital controller. A control algorithm that is suitable for regulating the multiple variables in the hybrid system is described by using a state-machine-based model; the issues about embedded control implementation are addressed; and the large-signal behavior of the hybrid system is analyzed on a voltage–current plane. The hybrid power source is then tested through simulation and validated on real hardware. This paper also discusses some important issues of the hybrid power source, such as operation under complex load profiles, power enhancement, and optimization of the hybrid system. The design presented here can not only be scaled to larger or smaller power capacities for a variety of applications but also be used for many other hybrid power sources.

Index Terms—Battery, digital control, fuel cell, hybrid power source, microcontroller, power capacity.

I. INTRODUCTION

FUEL CELLS have shown promising potential for several areas of applications such as those in portable electronics, hybrid electric vehicles, remote communication facilities, remote-ground support stations, etc. [1]–[4]. However, many applications have a common characteristic in their load profiles, that is, they have a relatively low average power demand but a relatively high pulse power requirement. The typical pulse duration in these applications generally ranges from hundreds of milliseconds to minutes, with power levels depending on
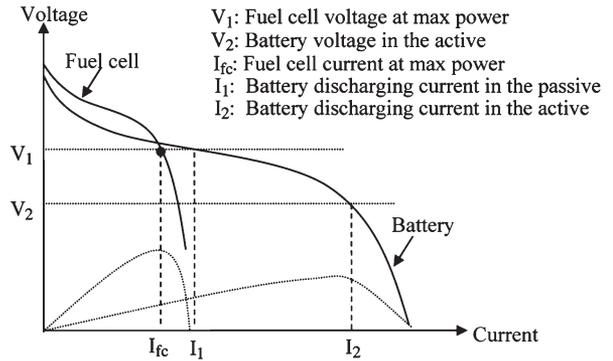
Fig. 1. Illustration of voltage–current (V–I) curves of the fuel cell and the battery showing that the output power capacity in the active hybrid is higher than that in the passive hybrid.

the applications. Fuel cell/battery hybrid power sources can meet these pulse power requirements with higher specific power and efficiency than the fuel cell alone while still preserving high energy density [5]–[11]. The simplest hybrid configuration, for example, passive hybrid, results from connecting both the fuel cell and the battery directly to the power bus [5]. However, this passive hybrid allows less flexibility in system design compared to the active hybrid that will be discussed below, because the nominal voltages of the fuel cell stack and the battery in the passive hybrid must be similar in order to not overcharge the battery, yet similar voltages then determine in a rather fixed way the amount of power that can be supplied from the fuel cell to the battery or to the load, as illustrated in Fig. 1.

As an alternative to the passive hybrid, a dc/dc power converter can be placed between the fuel cell and the battery so that they may have different voltage levels [6]–[11]. As shown in Fig. 1, the active hybrid can greatly augment the peak output power while not increasing the system weight and volume a lot, as will be discussed later. Active hybrid fuel cell power sources require a much more complex control scheme that must ensure efficient and robust power transfer from sources without risks of their rapidly degraded reliability due to prolonged overcurrent and/or undervoltage conditions. The power architecture and control scheme dedicated for hybrid fuel cell/battery sources must provide an uninterrupted power flow to the load. Therefore, rather than achieving a single voltage or current regulation goal at the output, the control system must regulate the power converter to balance the power flow of both sources so as to satisfy the load requirements while ensuring the various limitations of electrochemical components such as battery overcharge, fuel cell current limit (FCCL), etc.

Previous power controllers for hybrid power sources mostly employed complicated analog circuits [12]. Although analog
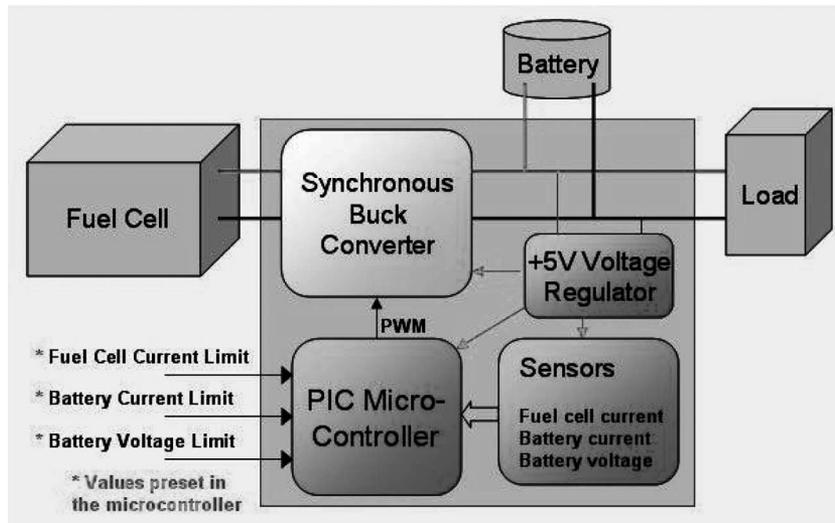
Fig. 2.   Digitally controlled fuel cell/battery hybrid power source.

control provides continuous processing of the signal, thus allowing a very high bandwidth, and gives infinite resolution of the signal measured, digital control is becoming attractive to modern power electronics controls due to many advantages over analog control such as programmability, less susceptibility to environmental variations, and lower parts count [13], [14]. Digital control allows designers to easily implement very complicated control algorithms such as that studied in this paper and to conveniently modify the control algorithm. It also reduces the size of the system by containing the complexity of the control system within the software. While conventional digital controllers based on discrete logic components require complex peripheral and auxiliary circuits [15], [16], a single-chip peripheral interface controller (PIC) microcontroller is used in this study to control the active hybrid power source.

This paper presents a compact digitally controlled fuel cell/battery hybrid power source based on a small number of parts. The architecture of the hybrid system and the implementation of the digital power controller are presented in Section II. In Section III, a control algorithm that is suitable for regulating multiple variables in the hybrid system is described by using a state machine model; the issues of embedded control implementation are addressed; and the large-signal behavior of the hybrid system is analyzed. The hybrid power source is then tested through processor-in-the-loop (PIL) simulation and validated on real hardware. Simulation and experiment results are given and analyzed in Section IV. Section V discusses some important issues regarding the hybrid power source, such as operation under complex load profiles, power enhancement, and optimization of the hybrid system.

II. DIGITALLY CONTROLLED HYBRID POWER SOURCES

A. Architecture of Active Hybrid Power Sources

In this study, the hybrid power source consists of a proton exchange membrane (PEM) fuel cell stack with a nominal power of 35 W, a lithium-ion battery, and a digital power controller, as shown in Fig. 2. This digital power controller circuit, which features smaller size and lighter weight compared to the conventional power controller, comprises a synchronous buck converter that is controlled by a PIC microcontroller, current and voltage sensors, and a voltage regulator that powers these components. The dedicated control software runs on the microcontroller. The user can set the FCCL, the battery current limit (BCL), and the battery voltage limit (BVL) in the control software. The control software coordinates the power converter for multiple objectives. The design presented here can not only be scaled to larger or smaller power capacities for a variety of applications but also be used for many other hybrid power sources.

B. Digital Power Controller

Fig. 3 schematically shows the architecture of the described digital power controller for fuel cell/battery hybrid power sources. The load is directly connected to the battery. The fuel cell is connected to the load through an H-bridge-based synchronous buck converter. An H-bridge chip operating in synchronous rectification mode is chosen as the chopper because it greatly reduces the parts count and can supply more current than a single traditional synchronous rectifier at the same ratings of the switches due to the two half-bridges in parallel. The battery provides additional power when the load needs high power and is charged by the fuel cell when the load is low. The currents from the fuel cell and to the battery are sensed by two current sense resistors and then amplified by the current amplifier. Since the resistance of each sense resistor is chosen as 0.1 Ω, and the gain of each amplifier is set as 10, the outputs of the current amplifier are the actual values of the currents measured. The voltage of the battery is measured by a voltage divider with a gain of 0.25 since the voltage range of the battery used in this study is from 10 to 16.8 V and the full dynamic range of the A/D converter is from 0 to 5 V. The measured fuel cell current, battery current, and battery voltage
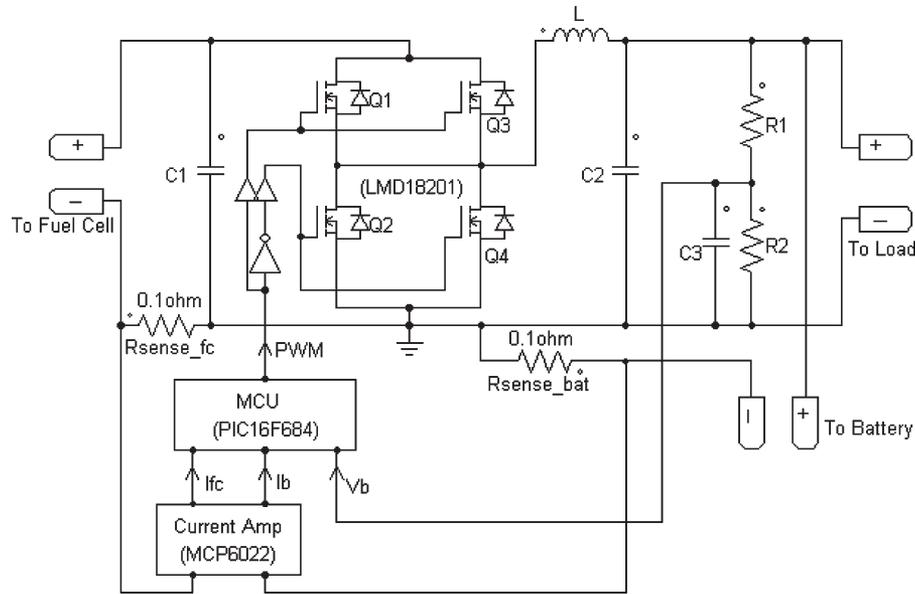
Fig. 3.   Architecture of the proposed digital power controller for the fuel cell/battery hybrid power source.

TABLE I
COMPONENTS USED IN THE DIGITAL POWER CONTROLLER

Component	Description
H-bridge chip	LMD18201
Microcontroller chip	PIC16F684
Current amplifier chip	MCP6022
Voltage regulator chip	LM140T-5.0
Power inductor	470uH
Input/output capacitors	110uF
Current sense resistors	0.1Ω

are fed into the digital controller that is implemented by a dedicated microcontroller (model PIC16F684). The PIC16F684 is a low-pin-count (14) 8-bit PIC Flash microcontroller with standardized features including a wide operating voltage of 2.0–5.5 V, on-board electrically erasable programmable ROM (EEPROM) data memory, and NanoWatt Technology. Standard analog peripherals include up to eight channels of 10-bit A/D, an analog comparator module with two comparators, programmable on-chip voltage reference, and an Enhanced Capture/Compare/Pulsewidth modulation (PWM) (ECCP). The ECCP peripheral offers up to four outputs with programmable dead band delay and autoshutdown and restart options.

FCCL, BCL, and BVL are preset by the users. The digital controller calculates the duty cycle of the buck converter based on the measured signals and produces a continuous PWM signal that is able to directly drive the H-bridge. Table I describes the components used in the power controller circuit. The digital power controller circuit has a very small size and is very lightweight, consisting of only four IC chips and a few passive components, where the power inductor dominates in weight and size.

III. EMBEDDED CONTROL SYSTEM

A. Control Strategy

The objective of the control software running on the microcontroller is to generate an appropriate PWM switching signal for the dc/dc power converter. By changing the duty cycle of the PWM switching signal, the output current of the fuel cell, the voltage, or the current of the battery can be regulated (but not independently). The control software for this system has three regulation modes, namely: 1) FCCL mode; 2) BCL mode; and 3) BVL mode. If the battery voltage exceeds the voltage limit, which may correspond to the condition of no load or light load coupled with high battery charge, the BVL mode applies. Under this mode, the output current of the fuel cell and the charging current of the battery should be below the rated currents. If the battery voltage is below the voltage limit, which may correspond to the condition of heavy load or light load coupled with low battery charge, the FCCL or BCL mode may apply depending on the load. If the current demand is lower than the rated output current of the fuel cell, the charging current of the battery may need to be regulated in order to protect the battery, i.e., the BCL mode is applied. In this case, the fuel cell current is unregulated but is always below the rated current. If the current demand is very high, the FCCL mode applies, and the fuel cell current is regulated at the limit (the rated current). In this case, the battery may be discharged or charged at a lower rate. If the battery voltage drops below a preset low value (low voltage disconnecting point), the load will be disconnected from the power source to protect the battery from overdischarging.

Fig. 4 shows the state machine representation of the control software. The blocks represent the regulation modes and the arrows show the event-triggered transitions between modes. These events happen under the corresponding conditions. For example, when the power source is first turned on, it works in FCCL mode. If there is no load or a light load, the charging
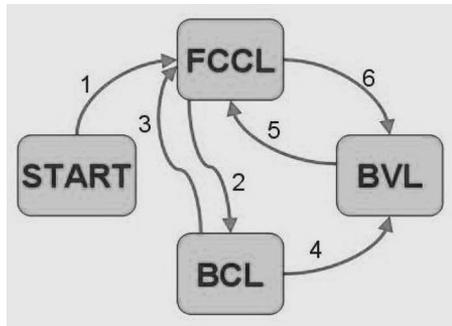
Fig. 4. State machine representation of the control algorithm for the fuel cell/battery hybrid power source.

Fig. 5. Block diagram of the control algorithm.

converter according to the selected regulation mode (control objective).

current of the battery may increase fast from zero to its limit, and then the BCL mode applies. When the battery voltage reaches the voltage limit, the BVL mode applies. Under either BCL or BVL mode, if the load increases very fast (i.e., when the fuel cell current reaches the limit), the FCCL mode will apply.

At any moment, the control strategy selects only one regulation mode. When any change in the fuel cell, the battery, or the load results in the satisfaction of the corresponding event condition, the controller will operate at another regulation mode. In the system shown in Fig. 2, the control strategy takes into account all the regulation modes and the conditions that result in the change of regulation mode. Under any condition of the load, the control strategy can decide the regulation mode correctly, as shown later in this paper. Thus, the control strategy is able to regulate the fuel cell current, the charging current, or the voltage of the battery by using only one control variable.

B. Embedded Control Implementation

The controller has three input variables, namely: 1) fuel cell current; 2) battery current; and 3) battery voltage, and two output variables, namely: 1) duty cycle of the power converter and 2) the enabling signal that can disconnect the load from the power source whenever the battery is overdischarged. Fig. 5 shows the block diagram of the control algorithm. The main functional modules in the controller code are the mode selection module and the compensation loop module. The mode selection module realizes the control strategy shown in Fig. 4 and outputs the regulation mode selected and the enabling signal for disconnecting the load as necessary. The regulation mode is determined according to the present operating conditions (the previous regulation mode and the measured currents and voltage) and the logic of the control strategy. The compensation loop module is used to compute the duty cycle of the power
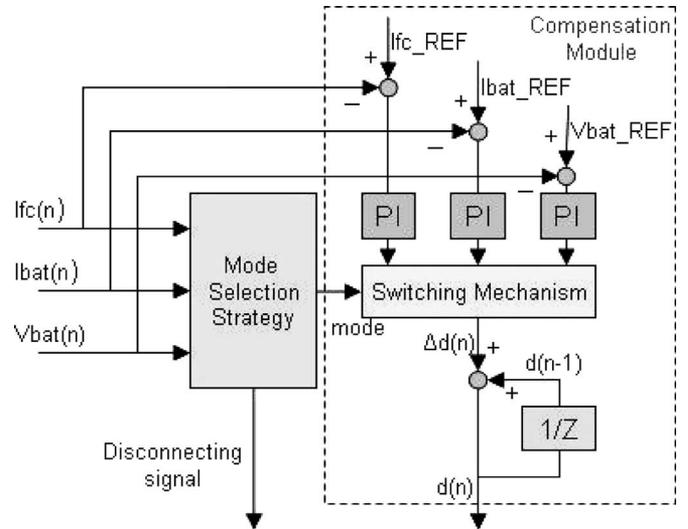
A modified proportional–integral (PI) approach is used to regulate the currents and voltage. The controller has different compensation objectives when different regulation modes are selected. In order to reduce the voltage or current transients that may occur when the regulation mode is changed, the control scheme consists of a feedforward term (implemented by the duty cycle at the previous sample interval) plus the proportional and integral terms of the errors of the currents or voltage. The duty cycle at the previous sample interval was stored in memory for calculation of the duty cycle at the present step. The proportional and integral terms of the errors are actually compensating the change of the duty cycle (Δd) at the present step. By doing this, the duty cycle will not change a lot at the time of mode change, and both the fuel cell current and the battery current can be regulated within the limits, even if transitions 2 and 3 may potentially be oscillatory when $I_{\text{bat\_REF}}$ and $I_{\text{fc\_REF}}$ are not selected appropriately or if the load varies frequently, because the effect of the fuel cell current error on the change of the duty cycle is similar to that of the battery charging current error. Whenever the regulation mode is changed, each integrator is reset to avoid unusual current or voltage transients at the time of mode change. The current and voltage regulations are formulated as

$$d(n) = d(n-1) + k_{\text{pifc}} \left(I_{\text{fc\_REF}} - I_{\text{fc}}(n) \right)$$
$$+ k_{\text{iifc}} \sum_{k=0}^{n} \left(I_{\text{fc\_REF}} - I_{\text{fc}}(k) \right) \tag{1}$$

$$d(n) = d(n-1) + k_{\text{pi}} \left(I_{\text{bat\_REF}} - I_{\text{bat}}(n) \right)$$
$$+ k_{\text{ii}} \sum_{k=0}^{n} \left(I_{\text{bat\_REF}} - I_{\text{bat}}(k) \right) \tag{2}$$

$$d(n) = d(n-1) + k_{\text{pv}} \left(V_{\text{bat\_REF}} - V_{\text{bat}}(n) \right)$$
$$+ k_{\text{iv}} \sum_{k=0}^{n} \left(V_{\text{bat\_REF}} - V_{\text{bat}}(k) \right) \tag{3}$$

TABLE II
GAINS FOR CURRENT AND VOLTAGE REGULATIONS

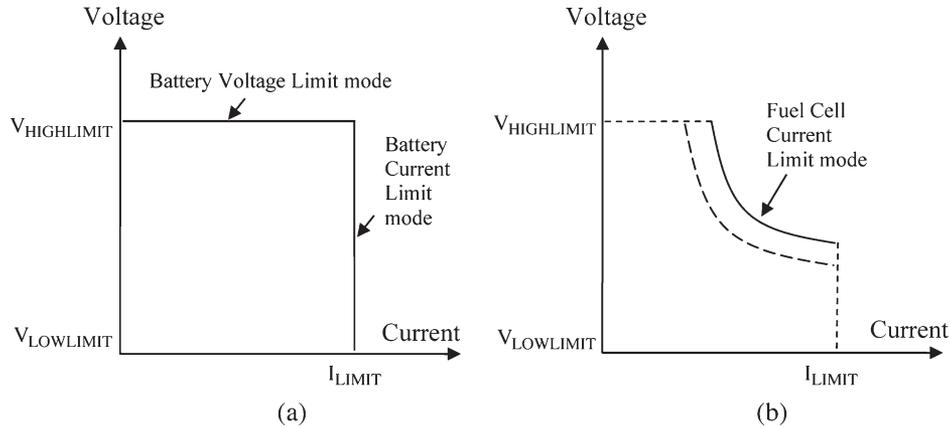| k_{pifc}	k_{iifc}	k_{pi}	k_{ii}	k_{pv}	k_{iv}
0.02 A^{-1}	1.0xe^{-5} (A.s)$^{-1}$	0.02 A^{-1}	1.0xe^{-5} (A.s)$^{-1}$	0.002V^{-1}	1.0xe^{-6} (V.s)$^{-1}$

Fig. 6. Analysis of the system behavior under different operation modes.

where I_{fc} is the sampled current from the fuel cell stack, V_{bat} the sampled voltage of the battery, I_{bat} the sampled current to the battery, $d(n)$ the duty cycles used to control the buck converter, $d(n-1)$ the value of the duty cycle left off the last time when the particular mode was engaged, I_{fc_REF}, V_{bat_REF}, and I_{bat_REF} the limits FCCL, BVL, and BCL, respectively, and k_{pifc}, k_{iifc}, k_{pi}, k_{ii}, and k_{pv}, k_{iv} the proportional and integral gains for the fuel cell current, battery current, and battery voltage, respectively. Since the modified PI control scheme contains the duty cycle value left the last time, the proportional term of the error may compensate the control in a way similar to the integral term in a traditional PI algorithm, and the integral gain in the modified PI algorithm does not necessarily have a large value, as does that in a traditional PI algorithm. The gains of PI compensation can be mathematically found by specifying the bandwidth and phase margin requirements of the loop gain or by placing the corresponding poles or zeros for the closed-loop system. Since the system transfer function is difficult to obtain and subject to change, the gains for both current and voltage regulations are manually tuned in this study by observing the system performances under the condition of ensuring system stability under different loads as listed in Table II.

C. Large-Signal Behavior

Due to changes of the load power demand and the battery state of charge, the control algorithm may force the system to frequently change from one operation mode to another. The need to ensure large-signal stability of the system may require some basic understanding of large-signal behavior of the system. In the following, the mode changes and the large-signal behavior of the system are analyzed.

When the system operates at BCL mode, the rest of the system, seen by the battery, appears as a constant current source, and the battery charging current is regulated at the current limit, as illustrated in Fig. 6(a), where the vertical axis represents

the battery voltage while the horizontal axis represents the battery charging current. In this mode, the operating point will move along the vertical line as the battery voltage increases, depending on the battery state of charge. The output power of the fuel cell depends on the load power requirement. When the system operates in BVL mode, the rest of the system, seen by the battery, appears as a constant voltage source, and the battery voltage is regulated at the voltage limit, as illustrated in Fig. 6(a). In this mode, the operating point will move along the horizontal line as the battery charging current decays. The output power of the fuel cell depends on the load power requirement.

When the load is increased such that the fuel cell current reaches the limit, the system will switch to FCCL mode. The output power of the fuel cell is constant since the current (or say, voltage) of the fuel cell is fixed by controlling the power converter. As mentioned before, if the load demand is low, the battery may be charged. Assuming that the load draws constant power within the time period we are interested in, the power transferred to the battery is constant, and the V–I curve of the battery is a constant power line, as shown in Fig. 6(b); thus, the battery current depends on the voltage. The battery power line will move leftward or rightward on the state plane when the load power changes (for instance, the dashed curve in Fig. 6(b) represents a different operating state than the continuous curve). If the load demand is so high that the battery discharges, the battery will provide an appropriate amount of current to compensate for the discrepancy between the fuel cell power and the load power, and the battery discharging current is unregulated.

The increase in the load may cause the system to change from BCL mode to FCCL mode. The transition trajectory can be described by a line (line 1) on the state plane, the slope of which is equal to the equivalent series resistance of the battery in magnitude, as shown in Fig. 7(a). As a result of the mode transition, the battery charging current may decrease, and
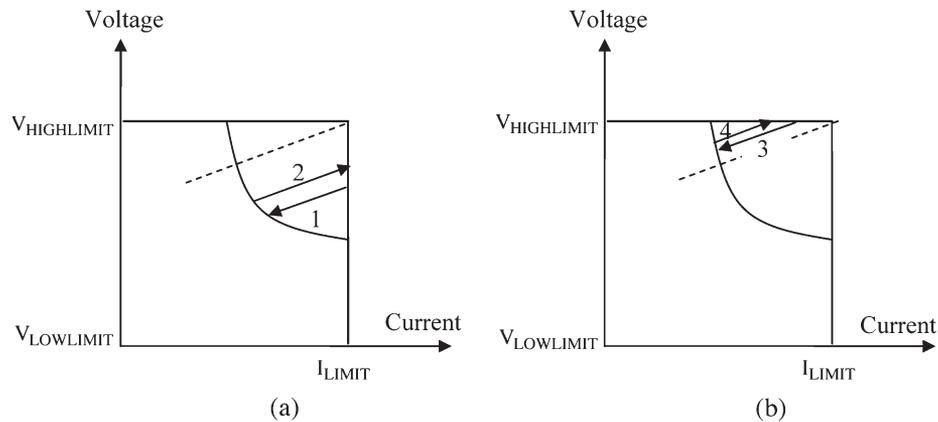
Fig. 7.   Analysis of the system behavior when the system changes from one operating mode to another.

consequently, the battery terminal voltage decreases slightly. In the reverse, when the system changes from FCCL mode to BCL mode, the transition trajectory can be described by another line (line 2) on the state plane. As a result, the battery charging current increases and so does the battery terminal voltage. Both the voltage and the current of the battery will experience a sudden change when the system changes from BCL mode to FCCL mode or the reverse.

The increase in the load may also cause the system to change from BVL mode to FCCL mode. The transition trajectory can be described by line 3 on the state plane, the slope of which is also equal to the equivalent series resistance of the battery in magnitude, as shown in Fig. 7(b). As a result of the mode transition, the battery charging current may decrease, and consequently, the battery terminal voltage also decreases slightly. In the reverse, when the system changes from FCCL mode to BVL mode, the transition trajectory can be described by line 4 on the state plane. As a result, the battery charging current increases and so does the battery terminal voltage. Both the voltage and the current of the battery will experience sudden changes when the system changes from BVL mode to FCCL mode or the reverse.

The transition from BCL mode to BVL mode is relatively simple, moving from the vertical line to the horizontal line at the cross point. Both the voltage and the current of the battery will experience a continuous change when the system changes from BCL mode to BVL mode.

IV. SIMULATION AND EXPERIMENT

A. PIL Simulation

In order to tune the controller parameters and to evaluate the controller performance, a processor-in-the-loop (PIL) simulation was first conducted in the Virtual Test Bed (VTB) [17]. The PIL simulation [18] is the first step taken to test the control algorithm in the embedded controller where the VTB simulates the plant model while the control algorithm runs on the microcontroller. At this stage, the VTB simulation model interacts with the microcontroller via a serial connection. At each time step, the VTB simulates the plant model for one sample interval and exports the system output to the microcontroller. When the microcontroller receives signals from the plant

model, it executes the controller code for one sample interval. The microcontroller returns its control signals computed during this step to the VTB via the same communications link. At this point, one sample cycle of the simulation is complete, and the plant model proceeds to the next sample interval. This stage of the design process is useful in determining the parameters for control of the plant.

Fig. 8 shows the VTB schematic view of the system presented in Fig. 2. The fuel cell model represented a 25-cell PEM fuel cell stack. The battery was configured as four cells in series and two strings in parallel. The nominal capacity of each cell was 1.4 Ah. The initial state-of-charge of the battery was 70%. A switching-average buck converter represented the H-bridge-based buck converter. The controller model was an interface to the microcontroller, which was responsible for exchanging data between the simulation and the hardware. The load drew a pulse current of period of 10 s. The low current was 0.1 A for 9 s, and the high current was 7 A for 1 s. This cycle was intentionally chosen for the purpose of investigating the performance of the described control strategy, but of course in practical applications, the power of the load might vary more randomly and not so regularly, as will be investigated later. FCCL, BCL, and BVL were set as 2.2 A, 2.0 A, and 16.8 V.

B. Experiment Setup

The active hybrid power source was also validated with actual hardware. A prototype of the digital power controller was developed, and the fuel cell/battery hybrid power source was built using an H-Power DS35 PEM fuel cell stack and a Sony18650 lithium-ion battery. The major equipments used in the experiment are given in Table III. Fig. 9 shows a photograph of the hardware prototype. The fuel cell stack had a nominal power capacity of 35 W and a nominal open-circuit voltage of 24 V. The battery was configured in the same way as in the simulation. The programmable electronic load continuously drew a current of 0.1 A for 9 s and 7 A for 1 s. FCCL, BCL, and BVL were set as the same values as those in the simulation.

C. Results

Simulation and experimental results are shown in Figs. 10–13. Fig. 10 shows the voltages of the fuel cell and the battery
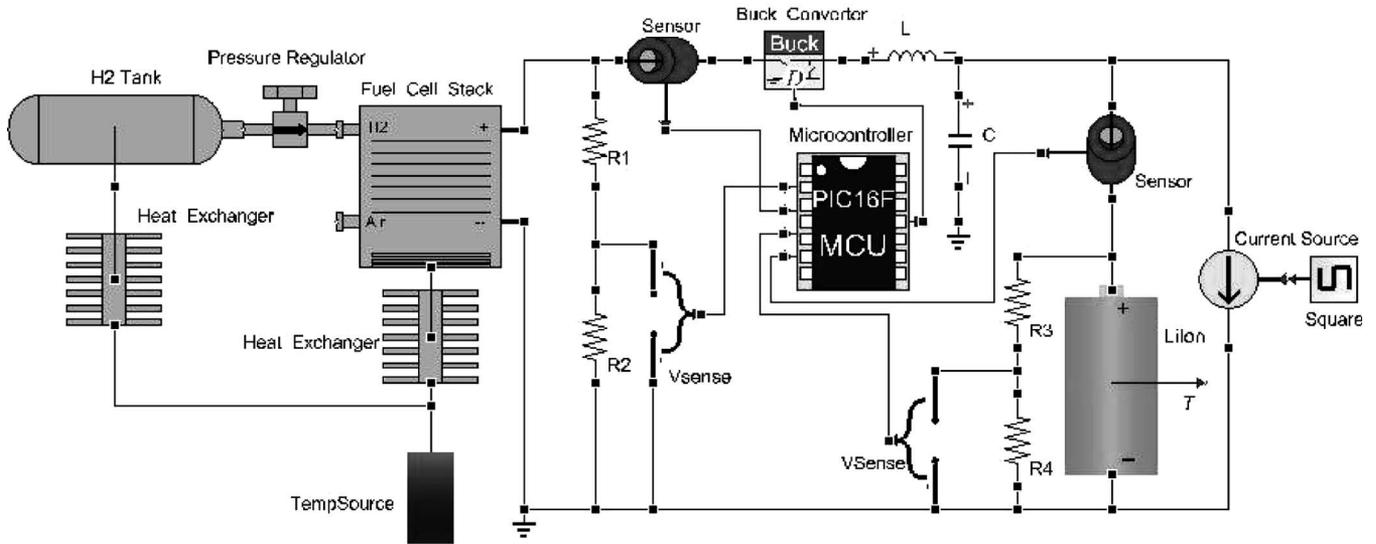
Fig. 8.   Schematic of the PIL simulation.

TABLE III
EQUIPMENT USED IN THE EXPERIMENT

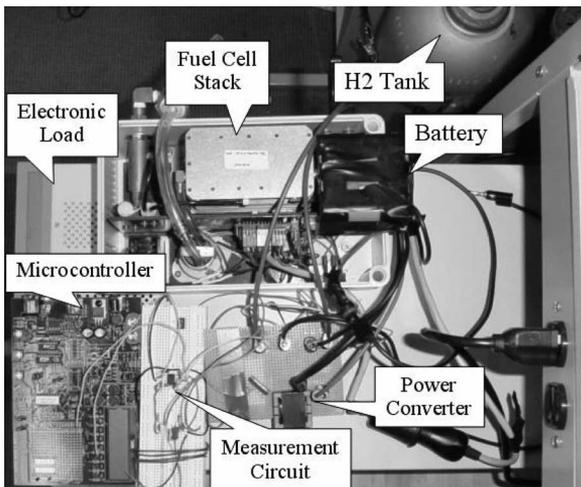| Component	Description	Number/Comment
PEM Fuel Cell Stack	H Power DS35	25 cells in series
Li-Ion Battery Pack	SonyUS18650	4 cells in series, 2 strings in parallel
Electronic Load	Chroma 6310	Digitally controllable
Power Controller	Developed	Digitally controllable

Fig. 9.   Photograph of the hardware prototype.

when the battery voltage was far below the limit. Fig. 11 shows the currents of the fuel cell and the battery in this case. Simulation and experimental results are plotted in the same figures for comparison. It is seen that when the load drew low power, the fuel cell stack provided current of about 1.8 A, supplying 0.1-A current to the load and charging the battery at 2.0-A current at the same time. In this case, the charging current of the battery was regulated (BCL mode applied), and the fuel

cell current was less than its limit. The fuel cell voltage was around 18.9 V, and the battery voltage was 16.2 V. When the load drew peak power, the fuel cell supplied a 2.2-A current. In this case, the fuel cell current was regulated (FCCL mode applied), and the discharging current of the battery depended on the load. At this time, the battery discharged at approximately 4.2-A current. The fuel cell voltage dropped to 17.4 V due to the higher current output, and the battery voltage dropped to 14.3 V. It is shown that the simulation outputs matched the experimental data very well. A slight difference between the measured voltages and the simulated voltages at high load current was observed. This was due to the small voltage drops on the current sensing resistors. The small difference between the measured and simulated battery currents at high load current might be caused by the slight inaccuracy of the sensing resistors. It can then be concluded that the experiment results validated the simulation model. It is seen that the currents of the fuel cell and the battery were regulated properly. It is also seen from the results that the fuel cell and battery currents experienced sudden changes as the mode changed between FCCL and BCL, as analyzed in the previous section.

Fig. 12 shows the voltages of the fuel cell and the battery when the battery voltage approached the limit. Fig. 13 shows the currents of the fuel cell and the battery. Simulation and experiment results are plotted in the same figures. When the load drew low power, the fuel cell stack provided about 1.9 A current (the current was a little higher than that in the previous
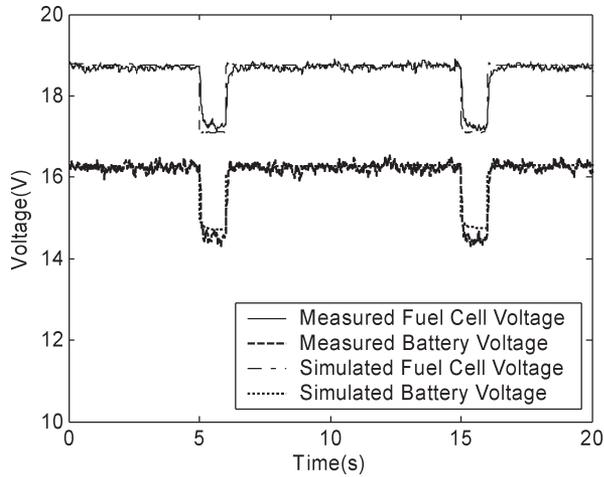
Fig. 10. Voltages of the fuel cell and the battery when the battery voltage was far below the limit.
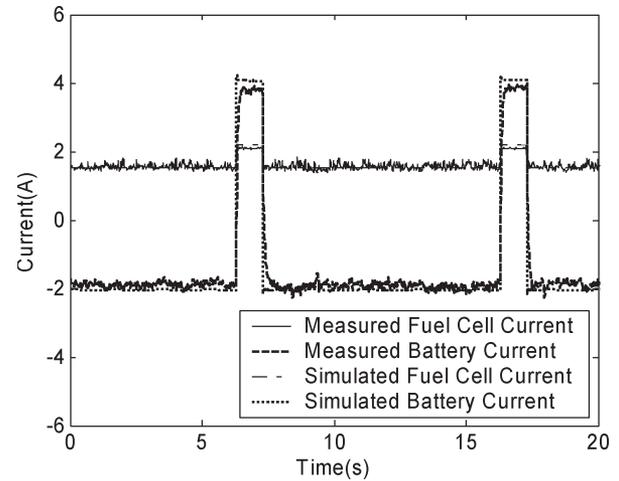

Fig. 11. Currents of the fuel cell and the battery when the battery voltage was far below the limit.

Fig. 12. Voltages of the fuel cell and the battery when the battery voltage approached the limit.
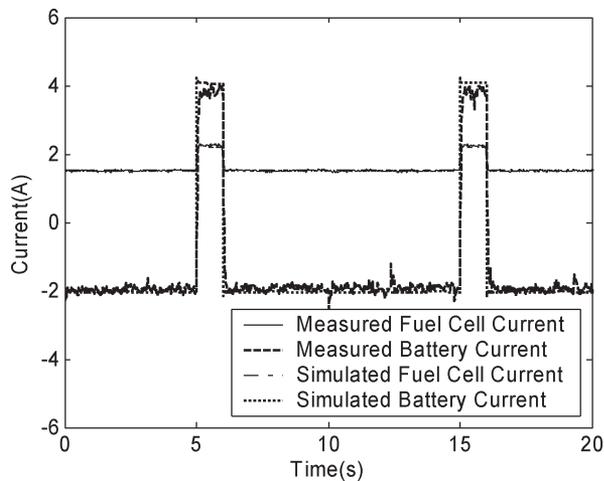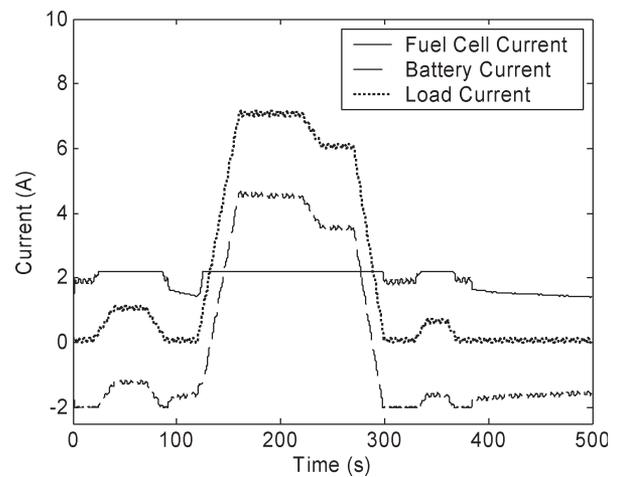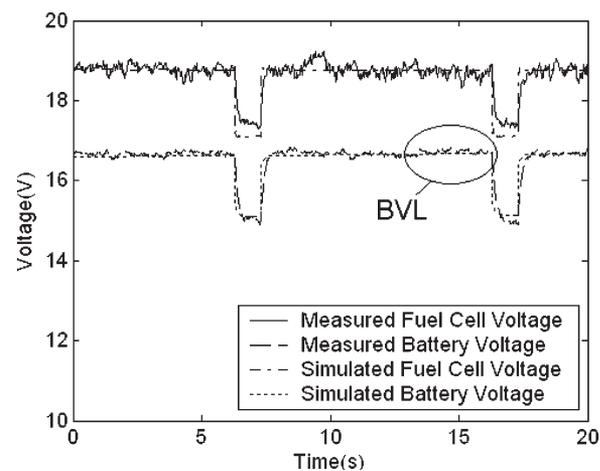
case because the battery voltage here was slightly higher and more power was charged to the battery), supplying 0.1-A current to the load and charging the battery at 2.0-A current at the same time. In this case, the charging current of the battery

Fig. 13. Currents of the fuel cell and the battery when the battery voltage approached the limit.

Fig. 14. Currents from the fuel cell, from the battery, and to the load.

was regulated (BCL mode applied), and the fuel cell current was less than the rated value (2.2 A). After a while (at about 12 s), the battery voltage reached the voltage limit (16.8 V). The BVL mode then applied, and the battery voltage was regulated at a constant level (see Fig. 12). The battery charging current decreased slightly, and so did the fuel cell current. It is seen from the results that both the battery voltage and the battery current experienced continuous and gradual changes as the mode changed from BCL to BVL, as analyzed in the previous section. These results show that the simulation outputs matched the experimental data very well. It is also shown that the battery voltage and the currents of the fuel cell and the battery were regulated properly.

V. DISCUSSION

A. Operation Under Complex Load Profiles

In order to test the control algorithm under more complex load profiles, the system shown in Fig. 8 was simulated under the load that drew a random current with peak current of up to 7 A, as shown in Fig. 14. There were some small fluctuations in the load current to represent the noise effect. The initial
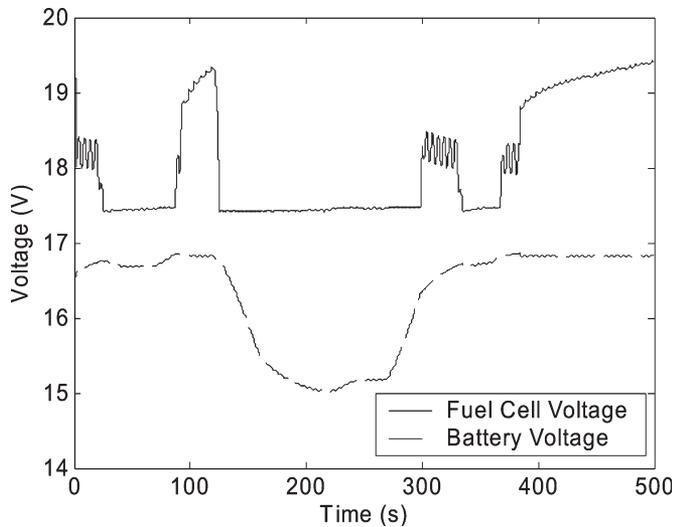
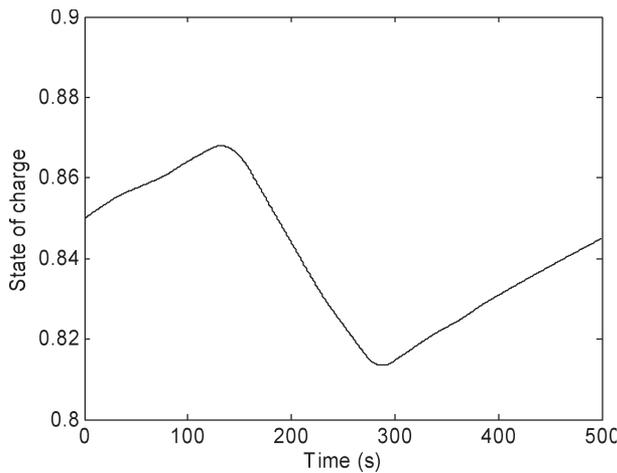Fig. 15.   Voltages of the fuel cell and the battery.

Fig. 16.   State of charge of the battery.

state-of-charge of the battery was 85%. FCCL, BCL, and BVL were set as 2.2 A, 2.0 A, and 16.8 V, respectively. Simulation results are shown in Figs. 14–17.

Fig. 14 shows that when the load initially drew a very small current, the fuel cell provided about 2.0-A current and the battery was charged at 2.0-A current (BCL mode applied). It is shown in Fig. 15 that the battery voltage increased gradually. When the load drew the first peak current, the FCCL mode applied, and the fuel cell supplied a 2.2-A current. At this time, the battery was charged at a lower rate (about 1 A). When the load demand decreased, the battery current was regulated at its limit. After a while, the battery voltage reached the voltage limit, and then the BVL mode applied. During the second peak duration, the fuel cell current was regulated at 2.2 A, and the battery was discharged at approximately 4.8 and 3.8 A, depending on the load. The battery voltage then dropped. When the load demand declined, the battery current was then regulated at the limit. The fuel cell supplied a 2.2-A current when the load demanded the third peak current. At the end of this cycle, the battery voltage reached the voltage limit, and the BVL mode was applied.
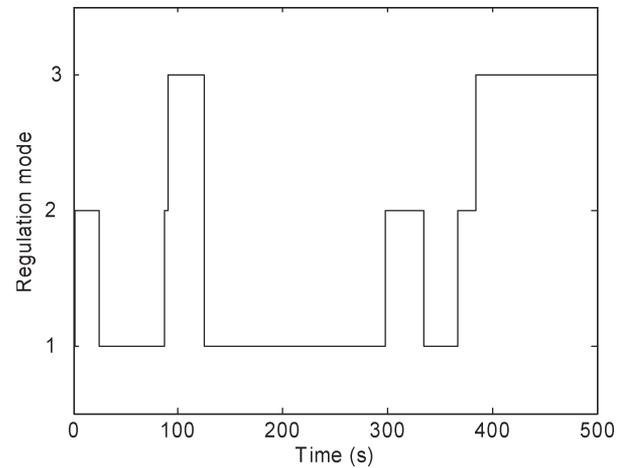

Fig. 17.   Regulation modes. (1) FCCL. (2) BCL. (3) BVL.

The state of charge of the battery, as shown in Fig. 16, increased when the battery was charged and decreased when it was discharged. During the studied cycle, the net increase of the state of charge was negative. This is because the average power of the load was a little higher than the output power of the fuel cell and the net input power to the battery is negative. Fig. 17 shows that the regulation mode was selected correctly according to the battery charge level and the load characteristics. Simulation results also suggest that the fuel cell current, battery current, and battery voltage were regulated properly under complex load conditions.

B. Power Enhancement

It is shown in Fig. 12 that when the load drew a peak current, the power source sustained a voltage between 14 and 15 V at the output terminal. The load drew from the hybrid power source about 101.5 W (14.5 V $\times$ 7 A) of power (shared by the fuel cell and the battery), which was much greater than the maximum power available from the fuel cell stack (35 W). It is worthwhile to note that the hybrid power source used in the experiment did not achieve the actual maximum power capacity. Considering the safe discharging range of the battery, the hybrid power source was tested at the maximum output. Table IV summarizes a comparison of three power sources, namely: 1) fuel cell alone; 2) passive hybrid; and 3) active hybrid in terms of system weight, volume, peak power capacity, and power density. Note that in the passive hybrid, five lithium ion cells are connected in series in order to match the fuel cell voltage.

It can be seen that the specific power of the active hybrid using an eight-cell battery is 1.7 times that of the passive hybrid and 3.5 times that of the fuel cell alone. It is clear that the active hybrid system with the addition of appropriate power electronics and controls is superior to the standalone component and the passive hybrid in terms of specific power.

C. Optimization

It is found from the experimental results that the efficiency of the hybrid power source (defined here as the energy delivered to the load divided by the energy from the fuel cell

TABLE IV
COMPARISON OF THREE POWER SOURCES

	Fuel Cell Alone	Passive FC/Battery Hybrid	Active FC/Battery Hybrid
System Configuration	Fuel Cell: H Power DS35	Fuel cell: H Power DS35 Battery: 5×2 (US18650)	Fuel cell: H Power DS35 Battery: 4×2 (US18650) DC/DC power converter
System Weight (g)	2900	3350	3266
Power capacity (W)	35	70	140
Specific power (W/kg)	12.1	20.9	42.9

during the period of interest, assuming that the final charge of the battery is at the same level as the initial charge) was higher than 92%, which makes the hybrid power source really attractive. The size was optimized according to power and voltage requirements. The objective was to achieve a power source with four times fuel cell power capacity and compatible voltage output. The fuel cell voltage was 17.3 V when in a maximum power output, so four lithium ion cells (with an average terminal voltage of 16 V) were connected in series to achieve a higher efficiency of the power converter since the battery voltage was compatible with the fuel cell voltage and the duty cycle was around 85%. When the load drew a peak power of 140 W, the battery needed to provide 105 W of power. Two strings of series-connected lithium ion cells were chosen to achieve such peak power, taking into account the safe discharging current of the lithium ion cell (4 A for one cell).

It is worthwhile to note that the size of each component in the hybrid power source such as fuel cell, battery, and power converter could be optimized in a global sense to achieve maximum system efficiency, which is beyond the scope of this paper.

VI. CONCLUSION

This paper has presented a compact digitally controlled fuel cell/battery hybrid power source. Such a hybrid power source provides much higher peak power than each component alone while preserving high energy density, which is important and necessary to many modern electronic devices, through an appropriately controlled dc/dc power converter that handles the power flow shared by the fuel cell and the battery. Rather than being controlled to serve only as a voltage or current regulator, the power converter is regulated to balance the power flow to satisfy the load requirements while ensuring the various limitations of electrochemical components such as battery overcharge, FCCL, etc. Digital technology is applied in the control of the power converter due to many advantages over analog technology such as programmability, less susceptibility to environmental variations, and fewer part counts. The digital power controller circuit primarily consists of a synchronous buck converter that is controlled by a PIC microcontroller, with features of small size and lightweight. The user can set FCCL, BCL, and BVL in the digital controller. A control algorithm that is suitable for regulating the multiple variables in the hybrid system is described by us-

ing a state-machine-based model; the issues about embedded control implementation are addressed; and the large-signal behavior of the hybrid system is analyzed on a voltage–current plane.

The hybrid power source is then tested through simulation and validated on real hardware. Simulation and experiment results show that the control algorithm is able to correctly select the regulation mode and appropriately limit the fuel cell current, the battery charging current, and the battery voltage. This paper has also discussed some important issues of the hybrid power source, such as operation under complex load profiles, power enhancement, and optimization of the hybrid system. The design presented here can not only be scaled to larger or smaller power capacities for a variety of applications but also be used for many other hybrid power sources.

REFERENCES

[1] A. S. Patil, T. G. Dubois, N. Sifer, E. Bostic, K. Gardner, M. Quah, and C. Bolton, "Portable fuel cell systems for America's army: Technology transition to the field," *J. Power Sources*, vol. 136, no. 2, pp. 220–225, Oct. 2004.
[2] K. Morita, "Automotive power source in 21st century," *JSAE Rev.*, vol. 24, no. 1, pp. 3–7, Jan. 2003.
[3] L. Hedström, C. Wallmark, P. Alvfors, M. Rissanen, B. Stridh, and J. Ekman, "Description and modeling of the solar-hydrogen-biogas-fuel cell system in GlashusEtt," *J. Power Sources*, vol. 131, no. 1/2, pp. 340–350, May 2004.
[4] T. Ruberti, "Off-grid hybrids: Fuel cell solar-PV hybrids," *Refocus*, vol. 4, no. 5, pp. 54–57, Oct. 2003.
[5] T. B. Atwater, P. J. Cygan, and F. C. Leung, "Man portable power needs of the 21st century: I. Applications for the dismounted soldier. II. Enhanced capabilities through the use of hybrid power sources," *J. Power Sources*, vol. 91, no. 1, pp. 27–36, Nov. 2000.
[6] M. Nadal and F. Barbir, "Development of a hybrid fuel cell/battery powered electric vehicle," *Int. J. Hydrogen Energy*, vol. 21, no. 6, pp. 497–505, Jun. 1996.
[7] R. F. Nelson, "Power requirements for batteries in hybrid electric vehicles," *J. Power Sources*, vol. 91, no. 1, pp. 2–26, Nov. 2000.
[8] P. B. Jones, J. B. Lakeman, G. O. Mepsted, and J. M. Moore, "A hybrid power source for pulse power applications," *J. Power Sources*, vol. 80, no. 1/2, pp. 242–247, Jul. 1999.
[9] C. E. Holland, J. W. Weidner, R. A. Dougal, and R. E. White, "Experimental characterization of hybrid power systems under pulse current loads," *J. Power Sources*, vol. 109, no. 1, pp. 32–37, Jun. 2002.
[10] Z. Jiang, L. Gao, M. Blackwelder, and R. A. Dougal, "Design and experimental tests of control strategies for active hybrid fuel cell/battery power sources," *J. Power Sources*, vol. 130, no. 1, pp. 163–171, May 2004.

[11] L. Gao, Z. Jiang, and R. A. Dougal, "An actively controlled fuel cell/ battery hybrid to meet pulsed power demands," *J. Power Sources*, vol. 130, no. 2, pp. 202–207, May 2004.

[12] M. J. Blackwelder and R. A. Dougal, "Power coordination in a fuel cell-battery hybrid power source using commercial power controller circuits," *J. Power Sources*, vol. 134, no. 1, pp. 139–147, Jul. 2004.

[13] T. Kawabata, T. Miyashita, and Y. Yamamoto, "Digital control of three-phase PWM inverter with LC filter," *IEEE Trans. Power Electron.*, vol. 6, no. 1, pp. 62–72, Jan. 1991.

[14] S. Saggini, M. Ghioni, and A. Geraci, "An innovative digital control architecture for low-voltage, high-current DC-DC converters with tight voltage regulation," *IEEE Trans. Power Electron.*, vol. 19, no. 1, pp. 210–218, Jan. 2004.

[15] T. Chern, J. Chang, C. Chen, and H. Su, "Microprocessor-based modified discrete integral variable-structure control for UPS," *IEEE Trans. Ind. Electron.*, vol. 46, no. 2, pp. 340–348, Apr. 1999.

[16] E. Koutroulis, K. Kalaitzakis, and N. C. Voulgaris, "Development of a microcontroller-based, photovoltaic maximum power point tracking control system," *IEEE Trans. Power Electron.*, vol. 16, no. 1, pp. 46–54, Jan. 2001.

[17] T. Lovett, A. Monti, E. Santi, and R. Dougal, "A multilanguage environment for interactive simulation and development of controls for power electronics," in *Proc. IEEE 32nd Annu. Power Electron. Spec. Conf.*, 2001, vol. 3, pp. 1725–1729.

[18] Z. Jiang, R. Leonard, R. Dougal, H. Figueroa, and A. Monti, "Processor-in-the-loop simulation, real-time hardware-in-the-loop testing, and hardware validation of a digitally-controlled, fuel cell-powered battery-charging station," in *Proc. IEEE Power Electron. Spec. Conf.*, Aachen, Germany, Jun. 20–25, 2004, pp. 2251–2257.

Zhenhua Jiang (S'01–M'03) received the B.Sc. and M.Sc. degrees from Huazhong University of Science and Technology, Wuhan, China, in 1997 and 2000, respectively, and the Ph.D. degree from the University of South Carolina, Columbia, in 2003, all in electrical engineering.

He was a Postdoctoral Fellow at the University of South Carolina before joining the University of New Orleans, New Orleans, LA, as an Assistant Professor in 2005. His research interests include digital control of power electronics, fuel-cell power sources and systems, renewable energy, energy storage, hybrid power sources and systems, integration of distributed energy resources, and modeling and simulation of interdisciplinary systems.

Roger A. Dougal (S'74–M'78–SM'94) received the Ph.D. degree in electrical engineering from Texas Tech University, Lubbock, in 1983.

In 1983, he joined the University of South Carolina, Columbia. He is the Director of the virtual testbed project, a multidisciplinary multiuniversity effort to develop a comprehensive simulation and virtual prototyping environment for advanced power sources and systems, integrating power electronics, electromechanics, electrochemistry, and controls into a common testbed. VTB is unique in allowing the simulation of multidisciplinary systems by importing models from discipline-specific source languages to a common workspace. In addition to modeling and simulation, his expertise includes power electronics, physical electronics, and electrochemical power sources.

Dr. Dougal received the Samuel Litman Distinguished Professor of Engineering Award and has been honored as a Carolina Research Professor.